Postprint

# THERMOMECHANICAL PROPERTIES AND PERFORMANCE OF CERAMIC RESONATORS FOR WIRELESS PRESSURE READING AT HIGH TEMPERATURES

P. Sturesson[1, 2, 3], Z. Khaji[2], S. Knaust[2], L. Klintberg[2], and G. Thornell[1, 2]
[1]*Ångström Space Technology Centre, Dept. of Engineering Sciences, Uppsala University, Uppsala, Sweden*
[2]*Div. of Microsystems Technology, Dept. of Engineering Sciences, Uppsala University, Uppsala, Sweden*
[3]*Div. of Military Technology, Dept. of Military Sciences, Swedish Defence University, Stockholm, Sweden*

Email: peter.sturesson@angstrom.uu.se

**Abstract** — This paper reports on the design, fabrication and thermomechanical study of ceramic LC resonators for wireless pressure reading, verified at room temperature, at 500 °C and at 1000 °C for pressures up to 2.5 bar. Five different devices were fabricated of high-temperature co-fired ceramics (HTCC) and characterized. Alumina green tape sheets were screen printed with platinum paste, micromachined, laminated and fired. The resulting samples were 21 x 19 mm$^2$ with different thicknesses. An embedded communicator part was integrated with either a passive backing part or with a pressure-sensing element, including an 80 µm thick and 6 mm diameter diaphragm. The study includes measuring thermally and mechanically induced resonance frequency shifts, and thermally induced deformations. For the pressure sensor device, contributions from changes in the relative permittivity and from expanding air, trapped in the cavity, were extracted. The devices exhibited thermomechanical robustness during heating, regardless of the thickness of the backing. The pressure sensitivity decreased with increasing temperature from 15 050 ppm/bar at room temperature to 2400 ppm/bar at 1000°C, due to the decreasing pressure difference between the external pressure and the air pressure inside the cavity.

***Keywords:*** **Wireless Reading, HTCC, Pressure sensing, Harsh Environments, Thermomechanical properties**

## 1. Introduction

In harsh environments, e.g., those of space exploration, geothermal research, and combustion engines [1, 2], high temperature, corrosive substances, high pressure and radiation are challenges for most hardware. MEMS devices and electronics are no exceptions.

Applications in high-temperature environments are numerous and related to various activities. They are specified differently depending on application. The military-grade temperature range for electronics is -55 °C to 125 °C [3]. There are commercial electronics claimed to be utilized for environments at temperatures up to 250 °C [4], and silicon oxide-based pressure sensors are reported to maintain performance at 300 °C [5].

Even higher temperatures are considered for a space exploration mission to the neighbouring planet Venus, where daytime surface temperature can reach 450 °C, and the atmospheric pressure can reach 90 bar [1]. The objectives for such a mission include determination of the composition of the surface, thus vehicles able to sustain such an environment are required [6]. In military jet engines, used in fighter aircraft, important parameters to monitor are temperature, pressure and gas flow [2]. The temperature is usually in the range of 15-1450 °C and the pressures typically range from 1 to 26 bar from intake to outlet, although exhaust

temperatures from jet engines reaching up to 1927 °C have been reported [7]. In volcanic research, the effusion rate of lava flow is an essential parameter for monitoring and predicting the volcanic eruption behaviour [8-9]. Lava usually exhibits a non-Newtonian flow state between 1000-1120 °C, which makes *in situ* measurements difficult [10].

However, already at At 600 °C, silicon, the most commonly employed MEMS material, deforms slowly if loaded mechanically [11]. Also, the electrical properties are affected. Wide-band semiconductors, such as single-crystalline aluminium nitride and silicon carbide can however be maintained up to around 800 °C [12].

High-temperature co-fired ceramics (HTCC) have temperature-stable electrical properties. HTCC alumina has a stable increase of the dielectric constant and is reported to exhibit stable electrical conductivity up to at least 600 °C [13]. Chen et al. have reported that the dielectric constant of 99.6% alumina is stable up to 550 °C at 1 MHz, after which it starts to increase [14]. Devices made from HTCC materials, which are fired at around 1500 °C, have been shown to sustain temperatures around 1000 °C [15], and alumina is mechanically stable to around 1100 °C [16]. Because of the high sintering temperature, a common conductor material is platinum, with the disadvantage of high resistivity, $10.6 \times 10^{-8}$ $\Omega$m, compared with that of silver, with $1.6 \times 10^{-8}$ $\Omega$m at room temperature [13].

Besides thermomechanical effects, such as thermal expansion and materials softening, the signal and power transmission by wire in high-temperature environments is challenging. From this perspective, it is beneficial to separate system components that do not sustain the required temperatures from those that do. Wireless reading from a low-temperature environment is one way to mitigate the challenge.

Signal transmission through wires can usually be substituted by wireless communication, Although powering is still an issue. Batteries operating at temperatures of 550 °C for 48 hours have been reported [17]. Recent developments suggest energy harvesting from, e.g., vibrations or thermal gradients [18], but the efficiency is low. Furthermore, if the conditions for harvesting vary, they not be able to power a device at any given time with a stable and continuous power unless energy can be stored in the device. However, devices may also be wirelessly powered. In the near-field domain, inductive coupling of magnetic fields between a sensor and a powering circuit can both drive and read a sensor. This is commonly used in RFID applications, and is studied as a solution for powering electrically driven automobiles, electrical devices and body-implanted devices [19-21]. However, the near-field domain will not be suitable for all environments that were mentioned above as they may require larger stand-offs than a near-field device allows.

Pressure sensing using ceramic devices is a well-stablished research field. Fonseca et al. have presented a micromachined wireless pressure sensor made of low-temperature co-fired ceramics (LTCC) with silver paste, for jet engine monitoring [22]. The sensor is designed as a passive LC resonating circuit with two capacitive diaphragms, and exhibits pressure sensitivities of 5387-9064 ppm/bar for external pressures up to 3 bars. Pressure sensing was demonstrated at room temperature, and a heat-induced frequency shift of 282 ppm/ °C, was measured up to 400 °C. The sensor showed stable performance over 24-hour periods. However, the signal loss due to decrease of the quality factor at higher temperatures, and the fact that the wired reader antenna was placed inside the pressure chamber, limited the maximum test temperature.

Radosavljevi et al. have reported an LTCC-based wireless pressure sensor for use in chemically aggressive environments [23]. The sensor is a fully embedded LC resonating circuit, and consists of a cavity having both a top and a bottom diaphragm. The resulting

pressure sensitivity at room temperature was 1183 ppm/bar for external pressures up to 3 bars above atmospheric pressure.

Xiong et al. and Tan et al. have demonstrated improvements of the work reported in [22], both in LTCC and HTCC [24, 25]. By applying a fugitive paste for support of the diaphragm during the fabrication, the yield was improved, and the resulting sensitivity of the LTCC sensor was 18163 ppm/bar at room temperature for pressures up to 3.6 bars. The temperature-induced frequency shift was measured up to 600 °C, and was 94 ppm/°C from room temperature to 500 °C, and 537 ppm/°C from 500 to 600 °C. The HTCC pressure sensors were fabricated of zirconia and alumina, with platinum as conducting material, and showed a pressure sensitivity of 9756 and 3140 ppm/bar, respectively, for pressures up to 4.5 bars. However, the devices were not characterized at elevated temperatures.

Recently, Cheng et al. reported on a wireless reflective patch antenna, made of sintered alumina and platinum paste, for use as a temperature sensor at temperatures up to 1050 °C [26]. Owing to the temperature-dependent relative permittivity of alumina, the sensor shifts its resonance frequency with 114 ppm/ °C from room temperature. They also reported on a evanescent-mode based resonating cavity pressure sensor, which was wirelessly read while, so far, being loaded with up to 5 N at temperatures up to 800 °C [27].

Also recently, Zhang et al. developed a wireless HTCC device, which was pressurized and read from at temperatures up to 800 °C. The device exhibits a sensitivity of about 17400 ppm/bar for pressures up to 1.9 bar. They also reported on a phase shift read-out system. [28]

In this paper, the thermomechanical behaviour of resonant LC circuit devices made of HTCC alumina with printed platinum conductors, for use in a pressure sensor node for instance and ultimately in jet engines, is studied. The reason is that the thermomechanical properties of the constituent materials vary, and that the device contains patterned parts. This may cause stresses and possibly mechanical deformation, making the device difficult to integrate with other components and systems. Also, it is of vital interest to study possible relationship between thermally induced deformation and performance.

An active reading system with a power-transmitting antenna is used to read the devices while they are being subjected to both heat and mechanical load. Furthermore, the deformation due to temperature increase is measured.

To demonstrate the integrability with a sensor element, one of the devices is furnished with a cavity sealed with a metallised diaphragm, which acts as a capacitor plate to enable wireless pressure readings at high temperatures. The work entails the design, fabrication and characterization also of this sensor node device.


## 2. Theory

Here, the theoretical basis for the design and operation of the devices is described.

### *Resonance Frequency*
An LC resonance circuit consists of an inductor in series with a capacitor. The resonance frequency, f, is described by

$$f = \frac{1}{2\pi\sqrt{LC}}, \qquad (1)$$

where $L$ is the inductance, and $C$ is the capacitance, which for a parallel plate capacitor is described as

$$C = \varepsilon_0 \varepsilon_r \frac{A}{d}, \qquad (2)$$

where $\varepsilon_0$ is the permittivity in vacuum, $\varepsilon_r$ is the relative permittivity for the dielectric material between the capacitor plates, $A$ is the capacitor plate area, and $d$ is the distance between the capacitor plates. The modified Wheeler model describes the inductance for a planar loop according to

$$L = K_1 \mu_0 \frac{n^2 d_{avg}}{1 + K_2 \rho}, \qquad (3)$$

where $n$ is the number of coil turns, $K_1$ and $K_2$ are design-related constants with values of 2.34 and 2.75, respectively, for square planar coils, $\mu_0$ is the permeability in vacuum, $d_{avg}$ is the mean value of the inner and outer length of the coil, and $\rho$ is the ratio of the difference and the sum of the outer and inner diameter, respectively [29].

*Pressure Sensor Element*
The sensing element consists of a diaphragm with a centred capacitor plate sealing a circular cavity. Pressure changes will cause the diaphragm to deflect and thus change the capacitance and the resonance frequency. For a flat circular diaphragm, the deflection, $\partial$, as a function of pressure is described by

$$\partial = \frac{3(1 - v^2) P a^4}{16 E h^3}, \qquad (4)$$

where, $v$ is Poisson´s ratio, $P$ is the ambient pressure, $a$ is the radius of the diaphragm, $E$ is Young's modulus, and $h$ is the thickness of the diaphragm [30]. The maximum stress, $\sigma_{max}$, during deflection is at the edge, and is described by [30] as

$$\sigma_{max} = \frac{3 P a^2}{4 h^2}. \qquad (5)$$

During sintering (described in detail in the next section), the material densifies and the cavity will be sealed at 1550 °C and at atmospheric pressure. As the sintered device cools down to room temperature, air trapped inside the cavity will contract to an extent corresponding to approximately 0.2 bar according to the ideal gas law, had the cavity been rigid. Here, the diaphragm will deflect corresponding to a subjection of a net external pressure of 0.8 bar. As the metallized layer is thin compared with the diaphragm, it will have a negligible influence on the deflection.

The corresponding stress in the diaphragm according to (5) is determined by the radius/thickness ratio squared. If the ratio is too large, the diaphragm will fail mechanically already during cooling from sintering. In any case, this bias of the diaphragm needs to be taken into account.

## 3. Design
The device is designed with a communicator part with either a mechanical backing part or a sensor element part attached to it. The communicator part consists of a square, 8-turn planar coil in series with a 4x4 mm² capacitor plate centred in the loop, figure 1 (left). Both the coil´s conductor width and isolation distance are 250 µm. Hence the coil pitch is 500 $\mu$m. The second capacitor plate, also 4x4 mm², is either placed on the passive backing part or on the diaphragm of the sensor element, figure 1 (right).
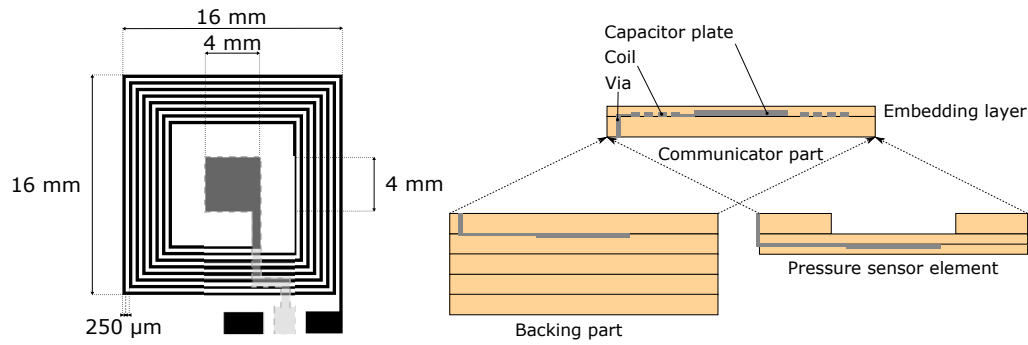
**Figure 1.** Top view of the top-layer of the device (left), and a cross-section schematic divided into: communicator part, backing part (the additional stack), and the pressure sensor element (right).

For the study of thermomechanical behaviour, three devices with a communicator part and varying backing part thicknesses were chosen, figure 1 (right). As a wired reference, one additional device was studied. For the pressure sensor device, a device with a communicator part and a pressure sensor element was studied. The chosen design parameters are listed in table 1.

**Table 1.** Device features and their design values. The devices are listed with devices 1-3S having backing parts of varying thicknesses, device 4SW being the wired reference and device 5P being the pressure sensor device.

| Feature | Design value |
|---|---|
| Coil width [mm] | 16 |
| Capacitor width [mm] | 4 |
| Conductor width [µm] | 250 |
| Coil pitch [µm] | 500 |
| Isolation distance [µm] | 250 |
| Cavity diameter [mm] | 6 |
| Diaphragm thickness [µm] | 80 |
| Conductor thickness [µm] | 10 |
| | |
| *Thicknesses* [µm] | |
| Device 1S | 280 |
| Device 2S | 760 |
| Device 3S | 880 |
| Device 4SW | 240 |
| Device 5P | 360 |

For a diaphragm with 6 mm diameter and 80 µm thickness, and with Young´s modulus of about 400 GPa and a Poisson´s ratio of about 0.24 [31], the stress after sintering is expected to be around 85 MPa. However, assuming some relaxation at the high temperature of the sintering, this is probably an overestimate. The typical yield strength of sintered alumina is around 267 MPa [31], which would allow an additional, external pressure of 1.5 bar at room temperature before the diaphragm fails. The diaphragm deflection after sintering will approximately be about 5 µm at the centre. For an applied external pressure of 1.5 bar, the deflection will be about 15 µm at the centre.

## 4. Materials and fabrication
Here the materials, equipment and fabrication are described. During sintering of the tapes, a shrinkage of 20 % is assumed. This is compensated for in the fabrication.

Three devices (1-3S) were fabricated from ceramic green tapes with 99.99% alumina (ESL 44007-150/50 μm, Electro Science Laboratories, USA), with platinum paste (ESL 5542) for electrical conductors, capacitor plates and the coil.

For the communicator and backing part, respectively, conducting patterns were screen printed on a 150 μm thick green tape through a 325-lines-per-inch mesh and dried for 15 minutes at 50 °C. Lamination was performed at 20 MPa and 70 °C for 20 minutes in a hydraulic laminator (RMP 210, Bungard, Germany). After this, a 400-μm diameter via was milled through the stacked parts using a 400-μm diameter RF end mill tool in a PCB plotter (Protomat S100, LPKF, Germany), and filled with platinum paste using a 0.25-mm diameter syringe needle. The filling was repeated three times, and the paste was dried at 50 °C for 30 min between each round. The communicator part was then covered with a 50 μm thick sheet. To vary the total stiffness of the different devices, 4 and 5, respectively, additional 150 μm thick sheets were added to the backing part of device 2S and 3S.

The complete stacks were again laminated at 21 MPa and 70 °C for 20 minutes. After the second lamination, the samples were contoured to 23×21 mm devices using a 0.2-mm diameter universal cutter tool in the PCB plotter.

As a wired reference to the wireless samples, a fourth device, 4SW, was fabricated using the same materials and following the same procedure but without the 50 μm thick embedding layer on the communicator part and without additional sheets to the support part. Instead a SMA connector was soldered onto the device.

The communicator part for the pressure sensor device was screen printed on a 150 μm thick sheet, as described in previous section, but using a different platinum paste (ESL 5574-A), with lower resistivity for better high-temperature performance. For the pressure sensing part, an 8-mm diameter cavity was milled out from a 150 μm thick sheet using the PCB plotter. Two 50 μm thick sheets with a screen printed 5x5 mm$^2$ capacitor plate embedded in between, was mounted over the cavity, providing a diaphragm with a nominal thickness of 100 μm. For mechanical support during lamination, an 8-mm diameter and 125 μm thick graphite fugitive insert (ESL 49000, Electro Sciences Laboratories, USA) was milled out and placed in the cavity.

For this device, an in-house built isostatic laminator was used to ensure hermetic sealing. The complete stack was encapsulated in a vacuum bag and then placed in a water-filled stainless steel container. The entire container was heated to 70 °C before the water inside the steel-container was pressurized to 210 MPa for 20 min, using a high-pressure pump (HPLC 515, Waters, USA). After lamination, the device was contoured like the other devices. For connection, the device edge, where connection pads from the communicator and support part are accessible, was cut to a clean and smooth surface, and platinum paste was deposited onto the edge surface connecting the two parts.

In the final fabrication step, all devices were fired in a high-temperature furnace (ECF 20/18, Entech, Sweden) following a temperature profile suited for removing organics in the green tape and all of the fugitive insert, and for sintering the alumina and platinum, figure 2.
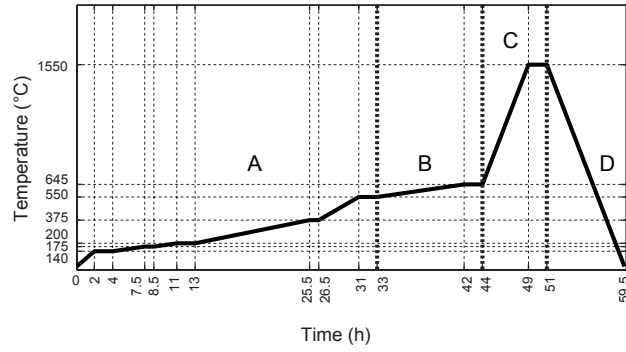
**Figure 2.** Firing profile for removing organic material and sintering. Region A represents removal of organic components in the green tape, region B represents the removal of the fugitive insert in the pressure sensing element, region C represents the sintering phase, and region D represents the cooling phase.

The stack build-ups, nominal values and design values of the devices are listed in table 2.

**Table 2.** List of device features, design values, shrinkage compensated nominal values, and the resulting green tape sheet stacks.

| Feature | Design value /Nominal value | Sheet stack build-up |
|---|---|---|
| Coil width [mm] | 16/19 | |
| Capacitor width [mm] | 4/5 | |
| Conductor width [μm] | 250/300 | |
| Coil pitch [μm] | 500/625 | |
| Isolation distance [μm] | 250/300 | |
| Cavity diameter [mm] | 6/8 | |
| Diaphragm thickness | 80/100 | |
| | | |
| *Thicknesses* [μm] | | |
| Device 1S | 280/350 | 50/150/150 |
| Device 2S | 760/950 | 50/150/150/4x150 |
| Device 3S | 880/1100 | 50/150/150/5x150 |
| Device 4SW | 240/300 | 150/150 |
| Device 5P | 360/450 | 50/150/150/50/50 |

## 5. Characterization
After sintering, all devices were inspected and measured with light microscopy and a thickness measurement gauge (ID-C112B, Mitutoyo Corp., Japan).

As an evaluation of general thermal sustainability, samples were heated using a butane flame, figure 3, and then powered and read from (described in detail below).
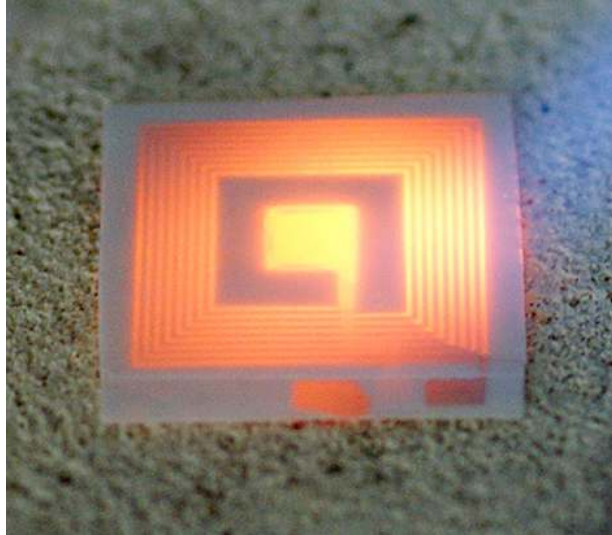
**Figure 3.** Butane flame heating of a device as a verification test before characterization.

The thermomechanical behaviour of devices 1-3S was studied by measuring the resonance frequency shift as a function of temperature as well as a function of deformation. Then the deformation as a function of temperature was studied. For the pressure sensor device, the resonance frequency as a function of temperature and as a function of pressure at different temperatures was studied.

*Thermomechanical evaluation*
In order to measure the heat-induced frequency shift, devices 1-3S were mounted, one at a time, in an alumina tube with a K-type thermocouple placed at the centre of the devices, and embedded with alumina sand giving increased thermal mass and uniform heat distribution. The setup was then heated slowly using a butane flame.

The devices were wirelessly powered and read using a loop antenna, here denoted reader antenna A, with a 90-mm diameter main loop made from a 4-mm diameter copper rod with a 20-mm diameter matching loop, milled out from a PCB board. For tuning the loop antenna to the frequency of the devices, a varactor diode (BB182, NXP, The Netherlands), controlled by an external voltage supplier, was employed. The capacitance was shifted in steps of 1.1 pF at every 0.625 s, allowing the resonance frequency of the loop antenna to be swept over the response signal of the device while the input port voltage reflection coefficient, $S_{11}$, was logged with a VNA (Fieldfox 9923, Agilent, USA). By plotting the minimum magnitude of the $S_{11}$ samplings, the resonance frequency of the devices was obtained as the maximum of the minimas, figure 4. This response was measured at room temperature, at 100 °C, and then in 100°C steps up to 700 °C, and at 750 °C, the highest temperature permitted by this setup.
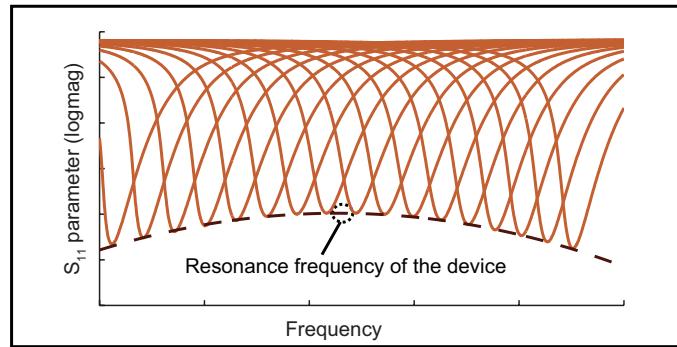
**Figure 4.** Frequency sweep of the loop antenna when placed 5 cm above a device. The resonance frequency of the latter is found at the maximum of the fitted line.

Platinum has a reported CTE of 8.94 ppm at 27 °C, and 11.96 ppm at 1000 °C [33] whereas alumina has a reported CTE of 4.6 ppm at 20 °C and 8.1 ppm at 1000 °C [32]. Mismatch in CTE between platinum and alumina might cause bimorphic mechanical deformation.

As the capacitor plates are parallel and centred on the devices, CTE mismatch in the capacitor is expected to have no contribution to buckling. The planar loop on the communicator part is not balanced by any platinum pattern on the backing side, and is therefore a potential source of deformation.

The resonance frequency dependency on mechanical deformation was measured on devices 1-3S and 4SW during three-point bending (AGS-X, Shimadzu, USA) with the load increasing from 0-10 N in steps of 0.5 N. Here, a different reader antenna, denoted antenna B, was used. Instead of a varactor, a trimmer capacitor was soldered to its main loop. The loop antenna was placed around the device. Device 4SW was powered and read through wire. All devices were connected to the VNA, logging the $S_{11}$ signal.

Knowing the resonance frequency dependency on mechanical deformation and measuring the heat-induced deformation of the devices will give the thermomechanical influence on performance. Therefore the thermally induced deflections of devices 1-3S were measured in an in-house fabricated laser profilometer. In this, a Kanthal–wired hotplate was mounted to a bi-axial translation stage, and a laser distance measurement system (OD5, SICK, Germany) mounted above it was used to measure the distance to the device while the platform was displaced in one direction with 0.5-mm steps. Each device was measured at room temperature and then at every hundred degrees up to 400 °C, the highest allowed temperature in the setup. The radius of curvature was extracted from the height profile with a curve-fitting algorithm, subtracting also the room temperature profile from those measured at higher temperatures.

*Pressure sensor evaluation*
To obtain the pressure induced resonance frequency shift, device 5P was placed inside a 600 mm long quartz glass tube, figure 5, with 2 mm wall thickness and an inner diameter of 27 mm and a fuse-sealed end. A brass flange with a stainless steel lid was connected to the open tube end using epoxy glue. The tube was pressurized through a 5-mm diameter polymer gas tube, connected through the stainless steel lid. For monitoring the temperature inside the tube, a K-type thermocouple was fed through the lid and into the quartz tube.

The sample was placed inside the tube, near the fuse-sealed end, and embedded in alumina sand for increased thermal mass and heat conduction. The thermocouple was mounted on the sample using ceramic high-temperature adhesive (Ceramabond 569, Aremco Products Inc, USA). For heating, an oxygen-acetylene gas flame was used. The flame was directed perpendicular to the tube to concentrate the heat and to avoid thermal radiation being transmitted through the quartz glass to the flange. The sample was wirelessly powered and

read from reader antenna A, being placed outside the tube. For heat shielding, the reader antenna was mounted on a 10 mm thick furnace insulation plate with an 80-mm diameter hole, centred inside the antenna loop. The hole in the shield allowed the antenna to be displaced along the tube, without being exposed to thermal radiation.
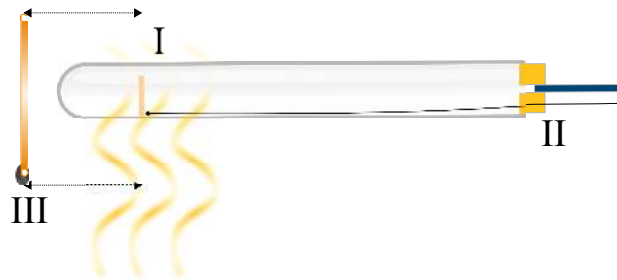


**Figure 5.** Drawing of the quartz glass furnace. The device with a posted thermocouple (I) is placed near the bottom of the tube, which is externally heated. Pressure is applied through the lid of the brass flange (II). The reader antenna (III) is moved between stand-by and reader position to minimize heating.

The heat-induced frequency shift of device 5P was measured at atmospheric pressure from room temperature and up to 1000 °C in steps of 100 °C. At room temperature, 500 °C and at 1000 °C, the temperature was kept constant and the tube was pressurized from atmospheric pressure, i.e 1 bar up to 2.5 bars in steps of 0.3 bar. Both the temperatures and pressures were stabilized before scanning. The pressure was monitored using a pressure gauge (PTI-S-AG10-32AO-Y, Swagelok, USA).

To study the influence of the expansion of the air trapped inside the cavity, the diaphragm was then perforated outside the capacitor plate using a 0.5-mm diameter diamond drill at 400000 rpm, and the resulting resonance frequency versus temperature was measured using the method described above for devices 1-3S, at atmospheric pressure.


## 6. Results

The lamination and firing of the samples resulted in a monolithic structure embedding the conducting pattern well. It was however observed that the conductors were pressed into the surface they were printed on.

All devices survived the evaluations, and maintained their performance after the temperature and pressure testing, except, of course, 5P, after the intentional perforation.

The resulting geometrical features of the devices exhibit values close to the design values, table 3.

**Table 3.** Comparison of the design values and the resulting feature values, and the resonance frequency at room temperature and atmospheric pressure after sintering.

| Feature | Design value | Resulted values | Resonance frequencies [MHz] |
|---|---|---|---|
| Coil width [mm] | 16 | 16.8 | |
| Capacitor width [mm] | 4 | 4.15 | |
| Conductor width [μm] | 250 | 252 | |
| Coil pitch [μm] | 500 | 504 | |
| Isolation distance [μm] | 250 | 252 | |
| Cavity diameter [mm] | 6 | 6.2 | |
| | | | |
| *Thicknesses* [μm] | | | |
| Device 1S | 280 | 285 | 45.1 |
| Device 2S | 760 | 760 | 46.2 |
| Device 3S | 880 | 890 | 43.3 |
| Device 4SW | 240 | 245 | 49.2 |
| Device 5P | 360 | 350 | 59.4 |

### *Thermomechanical evaluation*

The absolute thermally induced frequency shift, figure 6, at 750 °C was 103600 ppm for device 1S, 173700 ppm for device 2S and 133700 ppm for device 3S, respectively, showing a near-linear temperature coefficient for all devices. These three devices exhibit similar trends up to 500 °C, after which they diverge. For device 5P, the frequency shift follows a nearly linear trend, although with a lower temperature coefficient, and reaches a maximum of 46000 ppm at 1000 °C.
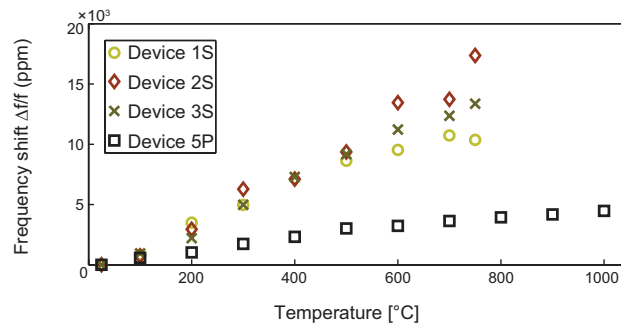


**Figure 6.** Absolute values of relative frequency shift as a function of temperature for devices 1-3S and for device 5P.

The wirelessly monitored mechanical deformation, figure 7, showed no resolvable shift for devices 1S and 2S until they reached a normalized radius of curvature of about 0.2 and 0.3 respectively. The maximum relative frequency shifts were -80 and -180 ppm, respectively. For device 3S, with values ranging between -20 and 40 ppm, no clear trend could be seen.
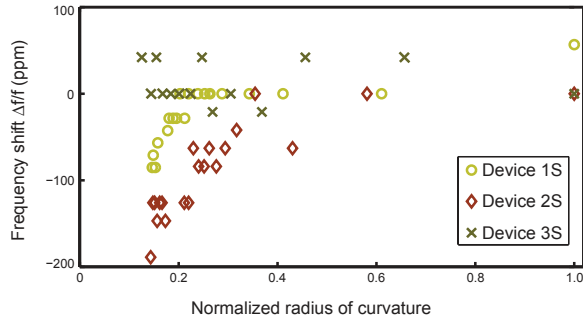
**Figure 7.** Relative frequency shift versus normalized radius of curvature from wireless reading. Normalized radius is defined as the ratio between the measured value and the initial radius of curvature.

For the wired device, 4SW, a similar behaviour was observed, albeit with a higher order of magnitude, with almost no frequency shift until a change of the normalized radius of curvature of about 0.2, figure 8. A maximum frequency shift of 56600 ppm was reached at the minimum normalized radius of curvature.
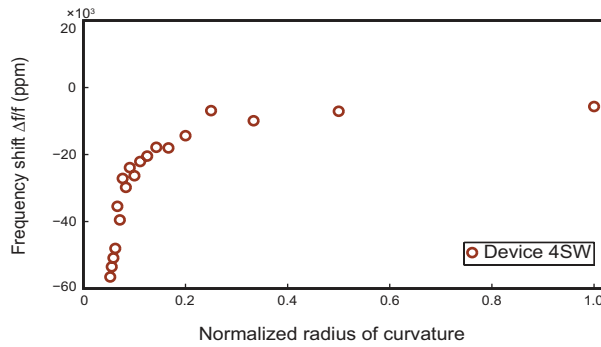


**Figure 8.** Relative frequency shift versus normalized radius of curvature from wired reading.

The heat-induced, normalized radius of curvature, figure 9, varied between 0.99 and 1.04 for device 1S, between 0.85 and 1.07 for device 2S, including the ill-behaved deformation at 200 °C, and between 0.98 and 1 for device 3S.
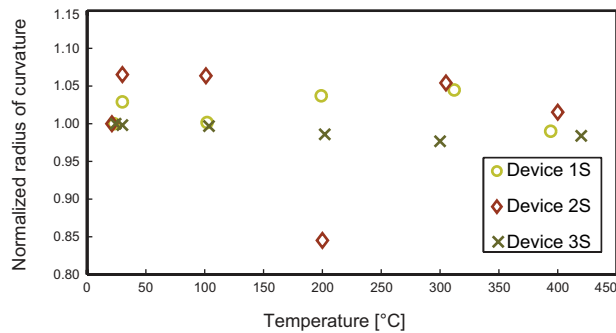


**Figure 9.** Normalized radius of curvature versus temperature.

*Pressure sensor evaluation*

At room temperature, the pressure-induced absolute relative frequency shift of device 5P is nearly linear with a sensitivity of about 15050 ppm/bar, reaching 22600 ppm at an external pressure of 2.5 bar, figure 10. At 500 °C, the device exhibits a lower sensitivity, about 8500 ppm/bar, than that at room temperature, and reaches 12100 ppm at 2.5 bar. At 1000 °C, the sensitivity is further decreased to about 2400 ppm/bar, and reaches 3500 ppm at 2.5 bar. The linearity of the sensor behaviour is somewhat decreased with increasing temperature.

The resonance frequency returned to its original value when the pressure was decreased to atmospheric pressure.
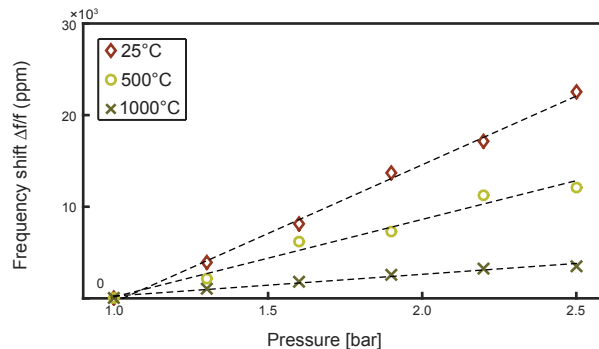


**Figure 10.** Relative frequency shift versus pressure from atmospheric pressure to 2.5 bars at room temperature, 500 °C and at 1000 °C for device 5P. The $R^2$ values are 0.99 for 25°C, 0.98 for 500 °C and 0.97 for 1000 °C.

The resonance frequency as a function of temperature for device 5P with a perforated diaphragm, figure 11, exhibited increased temperature sensitivity. It was also observed that the resonance frequency at room temperature had increased from 59.4 MHz to 59.8 MHz. The frequency shift previously reached at 1000 °C, was now reached already at 600 °C, and 56700 ppm was reached at 750 °C, figure 12. It is still a significantly smaller shift than for devices 1-3S.
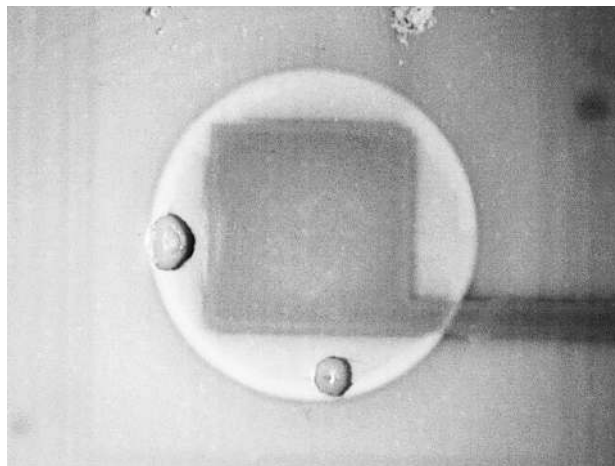


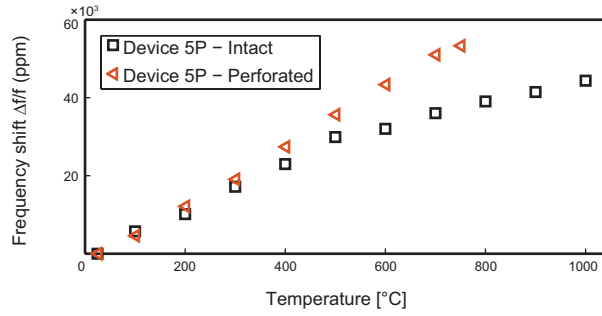**Figure 11.** Diaphragm of device 4 having been perforated with two holes.

**Figure 12.** Relative frequency shift as a function of temperature for device 5P before and after the diaphragm was perforated.

## 7. Discussion

This work presents a thermomechanical study on LC resonating devices, fabricated from HTCC, and reports wireless pressure sensing at 1000 °C. Device 5P exhibits a sensitivity that is slightly lower than the larger device presented in [28]. The decrease in pressure sensitivity with increasing temperature, observed in figure 10, is believed to be caused by a decreasing difference between the internal pressure in the cavity and the externally applied pressure. Mechanically, the diaphragm should be less stiff as Young's modulus decreases with increasing temperature [32].

The temperature-induced resonance frequency shift of devices 1-3S is substantial although the observed and calculated geometrical changes of the devices, as a function of temperature, are expected to contribute negligible to the resonance frequency shift. The geometrical contribution to the capacitance will be linear as the parallel plate area increases with a quadratic term and the plate distance with a linear term, equation 2. The inductance, equation 3, will grow linearly as it is only $d_{avg}$, which is a length. Hence, considering a well-behaved thermal expansion, the resonance frequency will be inversely proportional to temperature. Numerically, the thermally induced contribution, calculated from the resulting geometrical values of the devices and using equations 1-3, amount to approximately 4300 ppm at 750 °C, which is just a fraction of the observed shifts, figures 6 and 12. Instead, these frequency shifts are believed to be caused by changes in the relative permittivity. An extrapolation of data from [14] suggests a change from about 10.2 to about 12.5 between room temperature and 1000 °C and at 45 MHz. Subtracting the theoretically calculated thermally induced contributions, results in the suggested relative permittivity as a function of temperature displayed in figure 13.
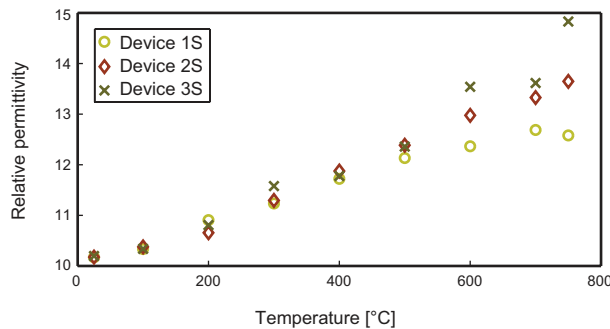


**Figure 13.** Relative permittivity of alumina around the resonance frequencies (approximately 45 MHz) for devices 1S-3S as calculated from the thermally affected resonance frequency after subtracting the theoretically calculated contribution from thermal expansion.

This strengthens the belief that the main driver of the thermal frequency shift is the relative permittivity. The deviation from linearity for device 1S, and to some extent also for device 3S that is observed in figures 6 and 13 is remains to be explained, however.

Bimorphic behaviour of the samples when heated is not observed. Variations of the normalized radius of curvature related to device thickness do not follow a clear trend but indicates a small deformation as the temperature increases. As the thickness ratio between platinum and alumina is small, the deformation is assumed to be governed by the deformation of alumina [33]. Regardless of thickness, it can be concluded that the devices are thermomechanically robust to 400 °C.

The influence on device 5P from diaphragm deformation, from cooling after sintering, is displayed in change of resonance frequency and in temperature sensitivity. The resonance frequency increased after the diaphragm was perforated, hence the counterbalancing between permittivity increase and expanding air in the cavity was removed, resulting in a higher temperature sensitivity as displayed in figure 12.

Frequency shifts in the wirelessly read relative resonance frequency during three-point bending are very small, figure 7, and resolvable shifts are observed at normalized radiuses of curvature that are far less than those that are observed as a function of temperature. For the wired device, 4SW, it is obvious that the resonance frequency shifts is larger than what is wirelessly measured, figure 8. However, it does follow a similar trend, indicating that the devices can be deformed significantly without affecting the resonance frequency, but also that the frequency eventually does shift abruptly when the deformation is large. Part of the difference in the results for wireless and wired measurements may be referred to quality factor differences between the reader antenna and the device, where the reader antenna does not follow the frequency shift of the devices accurately. It may also be a result of the vast presence of metal in the bending setup, close to the reader antenna.

A suggestion to future work would include studying and improving the performance of the wireless reading system including the reading antenna and the quality factor of the system. Initial results from wired devices connected to the VNA, with the same screen printed platinum conducting pattern as presented in this paper, exhibit quality factors of about 25.

## 8. Conclusions
- The first wireless HTCC pressure sensor has been demonstrated with pressure reading at 1000 °C..
- For the devices with varying thicknesses, the thermal frequency dependency is believed to be largely governed by changes in the relative permittivity of alumina rather than by geometrical changes.
- For the pressure sensor device, the air expansion, inside the cavity, reduces the heat-induced influence on the resonance frequency by the relative permittivity.
- The devices are shown to be thermomechanically stable, indicating a promising potential for integration and interfacing.

## References

[1]   Landis GA 2006, *Acta Astronaut*, **59,** 570-579

[2]   Spang III H A and Brown H 1999, *Control Eng. Practice*, **7,** 1043-1059

[3]   MIL-PRF-38534, *Test Method Standard,* (Columbus: DLA Land and Maritime)

[4]   Kappert H 2014 High Temperature SOI CMOS Technology Platform for Applications up to 250 °C, *High Temperature Electronics*, (Duisburg:Fraunhofer IMS), Germany

[5]   Toygur L 2012 A 300 °C Transimpedance Amplifier with Application to Capacitive Temperature Sensing *IEEE Sensors*, Taipei, Taiwan, 1-4

[6]   Del Castillio L, West W, Vo T, Hatake T, Mojarradi M and Kolawa E 2008, Extreme Temperature Sensing System for Venus Missions, *2008 IEEE Aerospace Conference*, Big Sky, USA, 2525-2531

[7]   Wilson, W C, Atkinson G M 2014, *IEEE Sensors Journal,* **14,** 3745-3753

[8]   Harris A J L, Dehn J and Calvari S 2007, *Bull. Volcanol* **70,** 1-22

[9]   Ganci G, Vicari A, Capello A and Del Negro C 2012, *Remote Sensing of Environment,* **119** 197-207

[10]  Pinkerton H, Norton G 1995**,** *J. Volcanic and Geothermal Research*, **59** 307-323

[11]  Domnich V, Aratyn Y, Waltrand M K, and Gogotsi Y 2008 *Rev. Adv. Mat. Sci.* **17** 33-41

[12]  Okojie R S, Lukco D, Nguyen V, and Savrun E 2015, *IEEE Electron Device Letters*, **36** 174–176

[13]  Fonseca M A 2007 Polymer/ceramic wireless MEMS pressure sensors for harsh environments: High temperature and biomedical applications, Sch. of El. And Comp. Eng. Institute of Technology, Atlanta, Georgia, p 74

[14]  Chen L Y 2005 Temperature Dependent Properties of Polycrystalline Aluminum Oxide Substrates with Various Impurities, *8$^{th}$ International Conference on Electronic Packaging (*Shanghai: IEEE), China

[15]  Lekholm V, Persson A, Palmer K, Ericson F, and Thornell G 2013 *,J. Micromech. Microeng.* **23** 055004

[16]  Carter C B, Norton M G 2007 *Ceramic Materials, Science and Engineering*, (New York: Springer) p 53

[17]  Ning X, Phadke S, Chung B, Yin H, Burke P and Sadoway D R, 2015, *J. Power Sources,* **275** 370-376

[18]  Köhler J E, Heijl R, Staaf L G H, Zenkic S, Svenman E, Palmqvist E C and Enoksson P 2013, *Proc. Royal Soc. Conf. Series,* **476** 012036

[19]  Villa J L, Sallán J, Llombart A and Fco Sanz, J 2009, *Applied Energy,* **86** 355-363

[20]  Kuipers J, Bruning H, Bakker S and Rijnaarts H 2012, *Sensors and Actuators A: Physical,* **178** 217-222

[21]  Chang C, Hou K, Shieh L, Hung S and Chiou J 2012, *Solid-State Electronics,* **77** 93-100

[22]  Fonseca M A, English J M, von Arx M, and Allen M G 2002 *J. Microelectromechanical Systems,* **11** 337-343

[23]  Radosavljevic G J, Zivanov L D, Smetana W, Maric A M, Unger M, and Nad L F 2009 *IEEE Sensors Journal* **9** 1956-1962

[24]  Xiong J, Zheng S, Hong Y, Li J, Wang Y, Wang W, and Tan Q 2013 *J. Zhejiang University-SCIENCE C (Computers & Electronics)* **14** 258-263

[25]  Tan Q, Kang H, Xiong J, Qin L, Zhang W, Li C, Ding L, Zhang X, and Yang M 2013 *Sensors* 13 9896-9908

[26] Cheng H, Ebadi S, Ren X and Gong H 2015 Sensors and Actuators A:Physical **222** 204-211

[27] Cheng H, Shao G, Ebadi S, Ren X, Harris K, Liu J, Xu C, An L, Gong X 2015**,** *Sensors and Actuators A: Physical*, **220** 22-33

[28] Zhang H, Hong Y, Liang T, Zhang H, Tan Q, Xue C, Liu J, Zhang W, Xiong J 2015, *Sensors* **15** 2548-2564

[29] Mohan, S S, del Mar Hershenson M, Boyd S P, and Lee, T H 1999 *IEEE J. Solid State Circuits* **34** 1419-1424

[30] M. Di Giovanni 1982 *Flat and Corrugated Diaphragm Design Handbook,* (New York: M Dekker INC) p 135-136

[31] Munro, R G, 1997, J. Am. Cer. Soc, **80** 1919-1928

[32] Kirby R K 1991, Int. J. Thermophysics., **12** 679-685

[33] Werdecker W and Aldinger F 1984 *IEEE Trans. Compon., Hybrids, Manuf. Technol.* **7** 399-404